Theoret. Appl. Mech., Vol.31, No.1, pp. 1-33, Belgrade 2004

Computer simulations of blood flow with mass transport through the carotid artery bifurcation

N.Filipović **M.Kojić** *

Abstract

The current paradigm for clinical diagnostic for the treatment of vascular disease relies exclusively on diagnostic imaging data to define the present state of the patient, empirical data to evaluate the efficacy of prior treatments for similar patients. These techniques are insufficient to predict the outcome of a given treatment for an individual patient. We here propose a new paradigm of predictive medicine where physician could use computational simulation to construct and evaluate a specific geometrical/anatomical model to predict the outcome for an individual patient. For this purpose it is necessary to develop a complex software system which combines user friendly interface, automatic solid modeling, automatic finite mesh generation, computational fluid dynamics and post-processing visualization.

The flow dynamics is defined according to the incompressible Navier-Stokes equations for Newtonian and non-Newtonian fluids. Mass transport of oxygen and macromolecules is modeled by the convection diffusion equation and coupled with flow dynamics. The computer simulations are based upon finite element analysis where the new computer methods for coupling oxygen transport and fluid flow are described.

The comparison results shows a good agreement between clinical observation for critical zones of flow separation, flow recirculation, low wall shear stresses which may contribute to the development of atherosclerotic diseases.

*Faculty of Mechanical Engineering, University of Kragujevac, Kragujevac, Serbia and Montenegro, e-mail: brckg@eunet.yu, fica@kg.ac.yu

Key words: Computer simulation, carotid artery, blood flow, mass transport, FE, surgical plans

1 Introduction

After heart disease and cancer, the third most common cause of death is stroke. Probably the most frequent stroke is of the embolic type with a heart disease as the source. The carotid bifurcation stenosis is also a significant cause of stroke, producing the infarction in the carotid territory by embolization or thrombosis at the site of narrowing, [1].

The carotid artery stenosis has a number of risk factors in common with other atherosclerotic diseases. In general, increase of stroke risk is induced by many factors: age, systolic and diastolic hypertension, diabetes, cigarette smoking, etc. However, it is still unknown how these risk factors contribute to the development of carotid territory stroke.

For patients with symptomatic carotid stenosis, the degree of stenosis appears to be the only predictive factor of importance in determining the stroke risk. On the other hand, asymptomatic patients have 'silent' stroke. Some authors found that only around 20% of asymptomatic patients had evidence of silent cerebral infarction which is visible on the computed tomography (CT). Symptomatic patients with carotid artery stenosis had significantly more CT verified lesions (47%).

According to above mentioned results, the following question arises: Is it possible to develop a software simulation that could predict predict carotid artery stenosis?

To answer this question it is necessary to investigate what we can get with today's computer techniques. The short- and long-term clinical outcomes of a carotid stenosis operation are very dependent upon the pre- and post-operative biomechanical and hemodynamical environment of blood flow through the carotid artery bifurcation. It is very difficult to generalize this environment because there is a wide variation between patients. The parameters such as the carotid geometry, the mechanical properties of the blood, and the nature of the clinical situation can vary widely.

Numerical analyses of the three-dimensional pulsatile flow through the carotid artery bifurcation have been published [2-11], among others.

There is a number of references on experimental flow investigations in the carotid artery, e.g. [12-16]. Some authors examined influence of the superior thyroid artery on the flow in carotid bifurcations, as reference [17], (we here neglect this effect), Delfino et al. [18] studied residual strain effects on the stress field of the carotid bifurcation.

The correlation between fluid dynamics and the localized genesis of atherosclerosis is known. There are many fluid dynamic factors which have influence on lesions in the carotid artery. Also the wall mechanics play an important role in artery collapse and plaque cap rupture ([19]).

.A numerical study of mass transport in large arteries was carried out by other authors [20-21]. To our knowledge, the mass transport phenomena have not been examined numerically in the carotid bifurcation. In the present work we give some results of this process.

To develop a realistic numerical simulation of the blood flow through the carotid artery bifurcation, it is necessary to model geometry of the carotid, incorporate the fluid properties of blood, calculate this complex system by finite element method (FEM), take relevant results and make the report for the clinicians.

We believe that only through the creation of such biomechanics based models it is possible to develop realistic surgical simulators that allow clinicians to explore and optimize the biomechanical consequences of surgery in a computer environment before stepping into the operating room. An ideal simulator for the carotid artery should allow the surgeon to investigate the consequences of surgical options, before performing the operation. A simulator with these characteristics requires the finite element analysis capabilities because of the complex patient-specific nature of the blood flow through carotid artery. With this approach the clinicians will be able to reduce the stroke risk in general.

Computer-generated simulations have become a very powerful tool in improving the clinical techniques. An important clinical benefit is to be gained by using the patient-specific computer simulations, since it is possible to explore the biomechanical consequences of surgical options before the first incision on the actual patient. The computer-visualized simulations allow a surgeon to predict zones of genesis of the atherosclerosis and tempo of development of already localized stenosis, with a

minimum amount of the user interaction. Also, this integrated software approach reduces the time to create blood flow computational model to hours instead of weeks.

A system of integrated software for quick creation of complex geometric model is presented in this work. The system consists of the automatic FE mesh generator, the finite element solver, and the scientific visualizer. Each part of the system represents an independent modulus organized in the object-oriented environment.

Because of the increasing size and complexity of the analysis and the software system design, a change in the programming approach and a shift in software design strategy have been proposed for developing readable, expandable and maintainable software systems. The change is from the procedure-oriented to object-oriented programming, and the shift is towards the object-oriented system development methodologies.

2 Graphical User Interface

The graphical user interface created for the carotid bifurcation is shown in Fig. 1. The interface system was designed to incorporate the anatomic model of the carotid artery for any patient. The user - vascular surgeon - can define the complete geometry of the mechanical model in a few steps. There are two standard types of techniques for determination of geometry for blood vessels. First, the arteriography has long been accepted as a standard method in determination of geometry of arteries. However, because of the cost and risk associated with the arteriography, the other less invasive methods for diagnosis and quantification of arteries have been suggested as alternatives. Within past several years techniques for measurement of stenosis have been developed using duplex ultrasonography and other ultrasound techniques. The ultrasound is an inexpensive, non-invasive diagnostic modality that can provide functional as well as anatomic information.

The next step is to transfer the main geometrical data in to a computer. There are several ways to do this. The completely automatic process would be a 3D shape reconstruction from arteriography or ultrasonography. We here use a parametric definition of geometry from

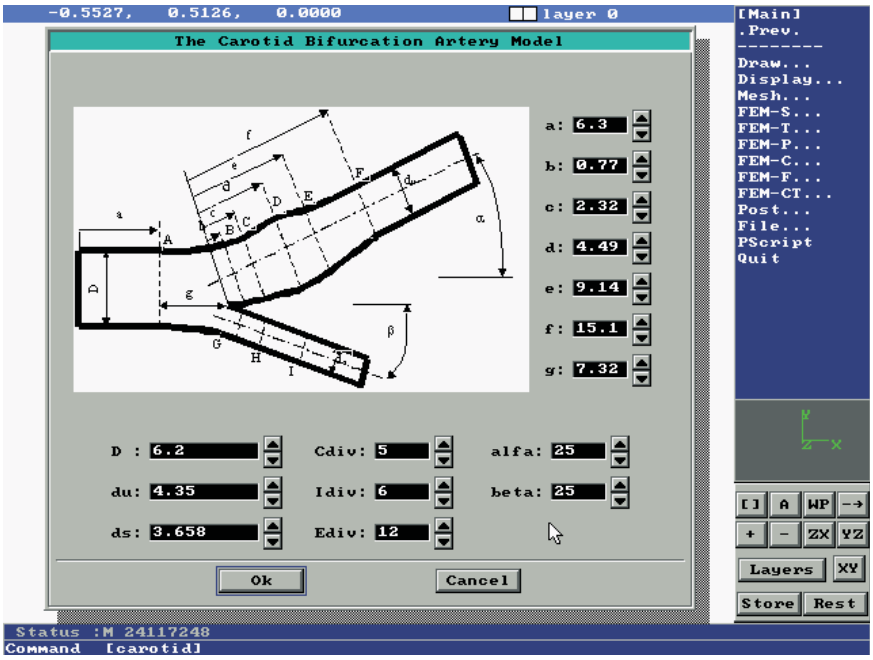

Figure 1: Graphical user interface with the main input parameters: D- diameter of common carotid artery, Du - diameter of internal carotid, Ds - diameter of external carotid, Cdiv, Idiv and Ediv are divison on the Common, Internal and External carotid artery respectively, alfa and beta are angles between internal and external with common carotid artery in the bifurcation symmetric plane, a, b, c,.., g are positions for different cross-sections of the model

Doppler ultrasound. It is self-automatic process where the clinician inputs more or less data for definition of the carotid geometry.

The user interface is organized, by default, as follows. There is a parametric input tool where the vascular surgeon should provide diameter of the common artery only. All the other variables are functions of the mean diameter of the common carotid artery. Another option is that surgeon inputs the mean diameters for common, internal and external carotid arteries as well as the sinus diameter. Of course, each diameter is subjected to change at any time.

Since very precise anatomic dimensions are needed for the FE model, this software can use input values for diameters at any distance along

the arteries. This assumes realistic presentation from Ultrasound device. Also, each cross-section can be changed independently. In order to construct very realistic model of vascular anatomy for carotid artery, the primitive forms such as circles, arcs, ellipses and splines are included in the software. Some of the cross-sections are shown in Fig. 2 as illustrations. The primitives are combined to generate the resulting surfaces used to define an enclosed, solid region (Fig. 3).

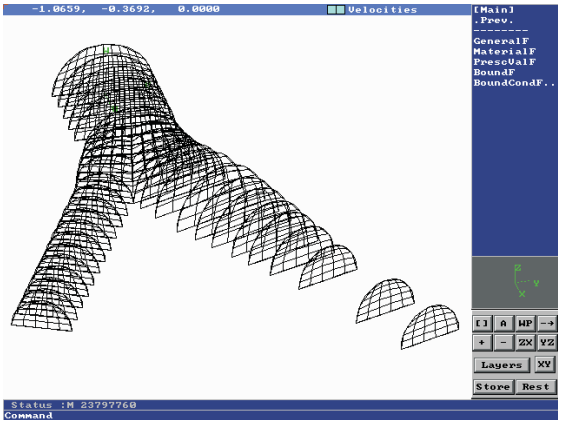

Figure 2: Definition of different cross-sections with 2D surface patches for one of the half of symmetric model

After defining the complete geometrical model, the simulator calls a program modulus for the FE mesh generation, [22]. This and the parts of the program that follow, are hidden from users. The mesh generation is perfomed automatically, but the user can affect it if he desires. Also, the boundary conditions are defined automatically, with the Re number at the entry of the common artery, where the fully parabolic velocity profile is assumed, as it is shown in Fig. 4. A complete FE model of carotid artery bifurcation is shown in Fig. 5.

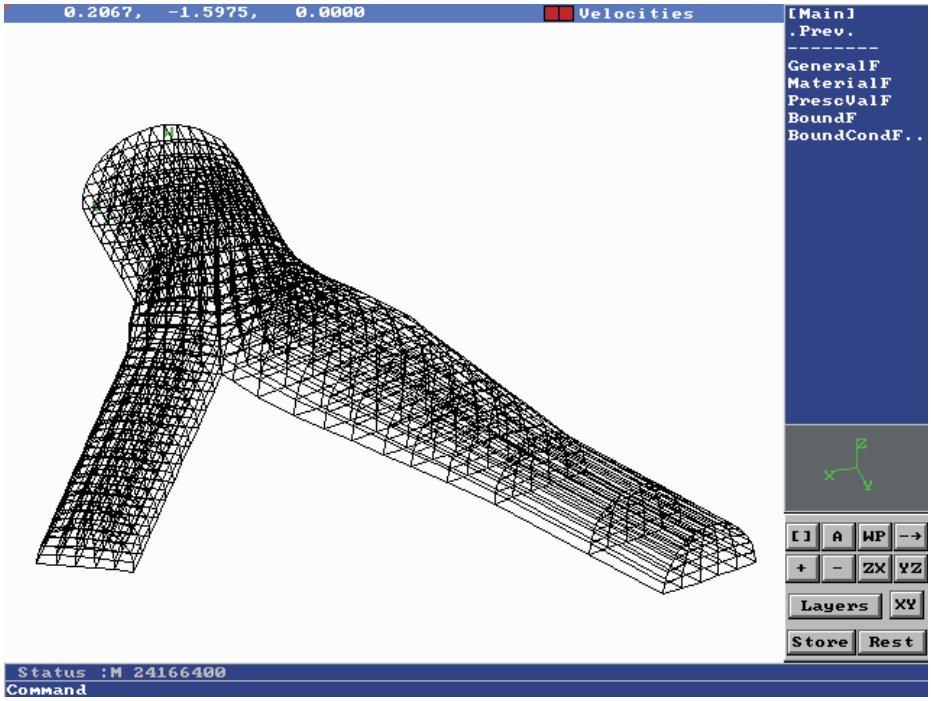

Figure 3: Making 3D finite element model

3 The Governing Equations Of Blood Flow And Mass Transport

3.1 Incompressible viscous fluid flow

The three-dimensional flow of a viscous incompressible fluid (such as blood) is governed by the Navier-Stokes equations that can be written as

$$\rho\left(\frac{\partial v_i}{\partial t}+v_j\frac{\partial v_i}{\partial x_j}\right)=-\frac{\partial p}{\partial x_i}+\frac{\partial}{\partial x_j}\left(\mu\left(\frac{\partial v_i}{\partial x_j}+\frac{\partial v_j}{\partial x_i}\right)\right) \tag{1}$$

$$\frac{\partial v_i}{\partial x_i}=0 \tag{2}$$

where v_i is velocity of blood flow in direction x_i, ρ is the fluid density, p

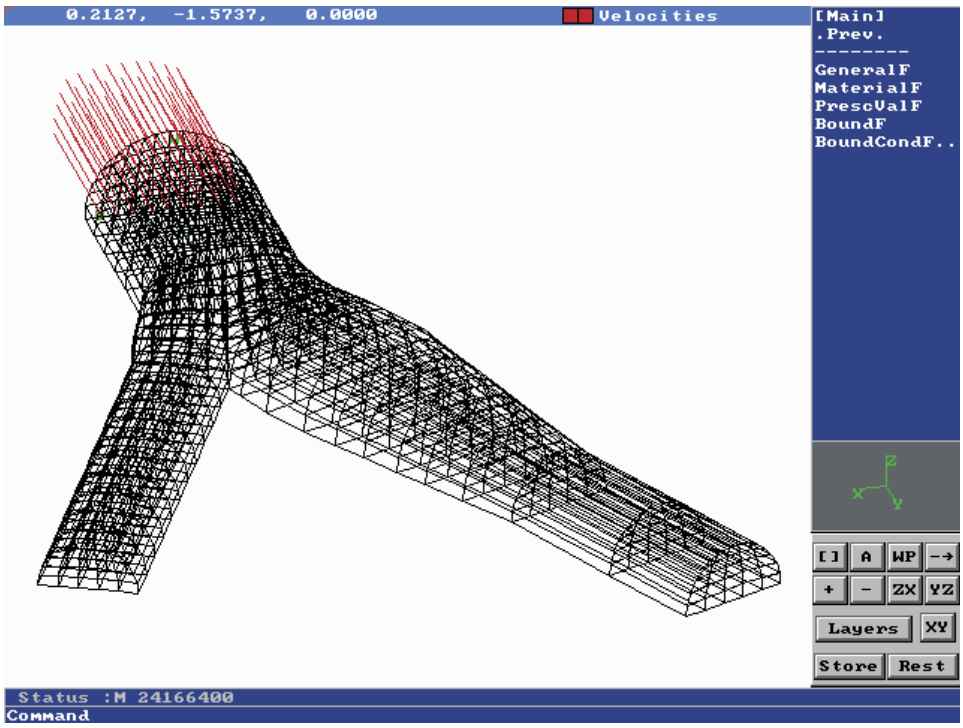

Figure 4: Prescribed input velocity at the entry of the common artery

is pressure, μ is the dynamic viscosity; and summation is assumed on the repeated (dummy) index, i,j=1,2,3. The first equation represents balance of the linear momentum of Newtonian and non-Newtonian inelastic fluids, while the equation (2) expresses the incompressibility condition.

3.2 Mechanical models of blood

Due to complex behavior of blood as a fluid, there are several blood models which are related to real flow in arteries. The models can be derived on Newtonian and non-Newtonian fluids. The Newtonian fluid has constant dynamic viscosity. On the other hand, the complex rheological properties of blood can be approximated by some of nonlinear non-Newtonian relations. The numerical simulation of hemodynamic flow needs the relationship between viscosity and shear rate. If one considers only the shear-rate-dependent viscosity of blood, then various

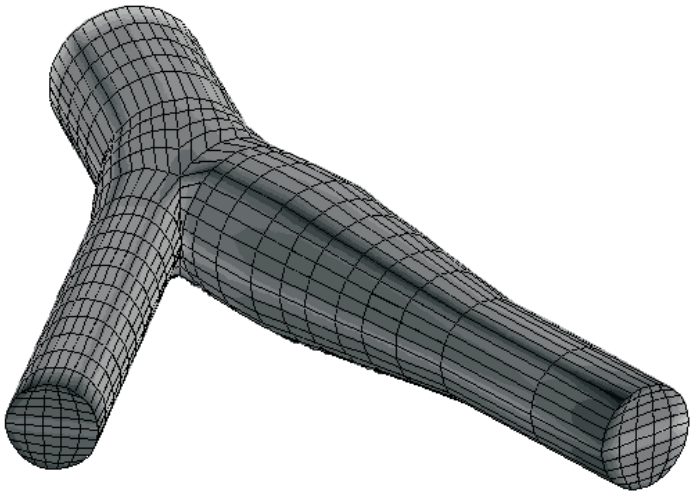

Figure 5: A complete FE model of the carotid artery bifurcation

constitutive equations developed to relate the shear stress tensor and the rate of deformation tensor can be utilized. A number of these constitutive equations have been used. The non-Newtonian viscosity of normal whole blood, measured by various investigators ([23]), is shown in Fig.6 as a function of the shear rate.

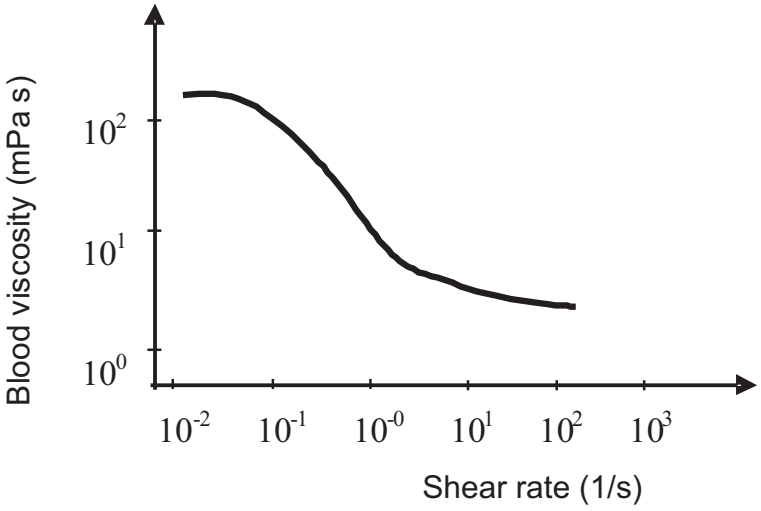

Figure 6: Blood viscosity vs.shear rate

In blood flow where the shear rates are not too low, the Casson's relation, based on the dynamic viscosity measurements is employed. The dominant factor affecting the behavior of blood as a suspension having the aggregatable particles, corresponds to the shear thinning effect at increased shear rates. The blood viscosity is derived as a function of the volume rate of particles-hematocrits, and of the shear strain rate. The generalized Casson relation, [3], is

$$\sqrt{\tau} = k_0\left(c_h\right) + k_1\left(c_h\right)\sqrt{2\sqrt{D_{II}}} \tag{3}$$

where k_0 and $k_1$are parameters depending on the volume fraction of particles in the suspension c_h, D_{II} is the second invariant of the strain rate tensor

$$D_{II} = \frac{1}{2} d_{ij} d_{ij} \tag{4}$$

with the strain rate components d_{ij} given as

$$d_{ij} = \frac{1}{2}\left(\frac{\partial v_i}{\partial x_j} + \frac{\partial v_j}{\partial x_i}\right), i, j = 1, 2, 3 \tag{5}$$

Finally, the dynamic viscosity μ is expressed as

$$\mu = \frac{1}{2\sqrt{D_{II}}}\left(k_0\left(c\right) + k_1\left(c\right)\sqrt{2\sqrt{D_{II}}}\right)^2 \tag{6}$$

A Newtonian constitutive model for viscosity was employed in the present study due to the fact that with non-Newtonian viscosity the differences are on the order of 10% [4].

3.3 The mass transport

The metabolism of the artery wall is critically dependent upon its nutrient supply. Oxygen is probably the most critical metabolite. Also oxygen is supplied to the cells of the avascular tissue layer by diffusion. The arterial blood flowing within the vessel lumen and the blood flowing within the vasa vosurum are two sources of oxygen.

Abnormalities in arterial wall oxygen tension have been implicated in the formation of atherosclerotic lesions. There are two forms of oxygen in blood: (1) free oxygen dissolved in plasma, and (2) bound to hemoglobin within red cells. Oxygen transport is a strongly nonlinear mass transfer problem because of the nonlinear dependence of oxyhemoglobin concentration on plasma oxygen partial pressure.

The mass transport is governed by convection diffusion equation

$$\frac{\partial c}{\partial t} + v_i \frac{\partial c}{\partial x_i} = k \left(\frac{\partial^2 c}{\partial x_i^2} \right) \tag{7}$$

where c denotes gas-concentration and k is the constant diffusion coefficient of the materials like gases (O_2, CO_2) or macromolecules (albumin, globumin).

Oxygen wall fluxes are frequently expressed in terms of the local Sherwood number, [24], Sh_D, which is defined as

$$Sh_D = \frac{q_w D}{D_b \left(PO_{2in} - PO_{2ref} \right)} \tag{8}$$

where q_w is the local wall oxygen flux, D is the arterial diameter, PO_{2in} and PO_{2ref} are the specified inlet and reference oxygen tensions, respectively. Relatively large Sherwood numbers are observed at the stenosis sites, consistent with high shear rates there.

3.4 The flow conditions

In order to determine the blood flow, the finite element analysis is carried out under physiological pulsatile conditions. The user-surgeon can prescribe flow waveforms in the common carotid artery and the phasic variation in the flow division ratio. Also, the user can define the duration of systolic and diastolic phases. Typical flow waveform in the common carotid artery, according to reference [2], is shown in Fig. 7. The ordinary pulse frequency is 75-80 strokes/min.

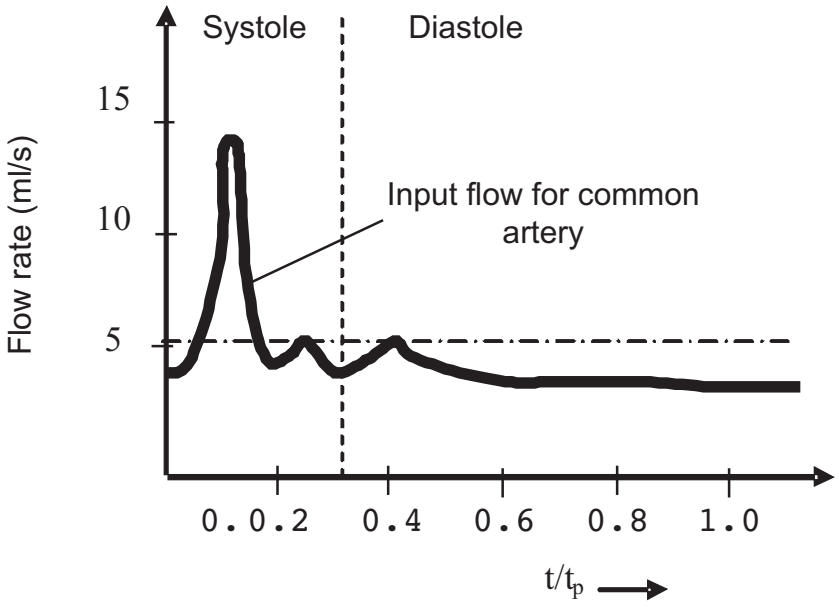

Figure 7: Flow waveform at the entry of the common carotid artery

3.5 Boundary conditions

At the inflow boundaries a fully developed flow in circular duct with given volume flux is prescribed. At the fixed walls all velocity components are prescribed as zero. Because the geometry on either side of bifurcation plane is the same for the model used, it is sufficient to consider only half of the bifurcation. In the plane of symmetry the velocity component normal to this plane and tangential stresses are imposed to be zero. At the ends of the internal and external carotid arteries, the outflow boundary condition is prescribed. The normal stress and both tangential stresses are set to be equal to zero (stress-free condition). This is an artificial boundary condition. Therefore near the outflow boundary, the solution differs from the solution in an infinitely long duct. Users can change the artery lengths in order to simulate physiological resistance at the ends of the arteries. Boundary conditions for mass concentration is prescribed constant concentration at the inlet of common carotid artery and no flux through the walls of the model.

4 Finite Element Procedure

Here we use specific coupling between mass transfer and fluid flow using penalty formulation with the following boundary conditions: prescribed inlet unsteady fluid flow as it is presented in Fig. 7. Boundary conditions for the transport equation is constant oxygen concentration at the inlet of the model, a symmetry condition $\partial c/\partial z$=0 at the plane symmetry and zero axial concentration gradient at the two outlet section downstream. The following are short descriptions of different formulation of finite element procedure implementing in the finite element software module.

4.1 Velocity and pressure formulation

For the solution of the nonlinear Navier-Stokes equations we have used two different formulations. The first is the velocity and pressure formulation, [25-27]. This formulation has many advantages because the pressure, velocity, velocity gradients and stress boundary conditions can be directly incorporated into the matrix equations.

The procedure of deriving the element equations relies on the Galerkin method, where the velocity and pressure fields are interpolated over the finite element.

For 3D analysis we use the 21/8 node element, where 21 nodes are employed to interpolate the velocities and 8 nodes are employed to interpolate the pressure. These interpolations provide stable elements as expresed by the inf-sup condition of Brezzi and Babuska, [28].

The incremental-iterative form of the equations for the time step and the equilibrium iteration "i" are:

$$\begin{bmatrix} \frac{1}{\Delta t}\mathbf{M_v} + {}^{t+\Delta t}\mathbf{K}_{\mathbf{vv}}^{(i-1)} + {}^{t+\Delta t}\mathbf{K}_{\mu\mathbf{v}}^{(i-1)} + {}^{t+\Delta t}\mathbf{J}_{\mathbf{vv}}^{(i-1)} & \mathbf{K_{vp}} \\ \mathbf{K_{vp}^T} & \mathbf{0} \end{bmatrix}$$

$$\begin{Bmatrix} \Delta\mathbf{v}^{(i)} \\ \Delta\mathbf{p}^{(i)} \end{Bmatrix} = \begin{Bmatrix} {}^{t+\Delta t}\mathbf{F}_{\mathbf{v}}^{(i-1)} \\ {}^{t+\Delta t}\mathbf{F}_{\mathbf{p}}^{(i-1)} \end{Bmatrix} \tag{9}$$

where the matrices and vectors are:

$$\mathbf{M_v} = \rho \int_V \mathbf{H}^T \mathbf{H} dV$$

$${}^{t+\Delta t}\mathbf{K}_{\mathbf{vv}}^{(i-1)} = \rho \int_V \mathbf{H^T} (\mathbf{H}^{t+\Delta t}\mathbf{v}^{(i-1)}) \nabla^T \mathbf{H} dV$$

$${}^{t+\Delta t}\mathbf{K}_{\mu\mathbf{v}}^{(i-1)} = \int_V \mu \nabla \mathbf{H}^T \nabla^T \mathbf{H} dV$$

$${}^{t+\Delta t}\mathbf{J}_{\mathbf{vv}}^{(i-1)} = \rho \int_V \mathbf{H^T} (\nabla \mathbf{H}^{t+\Delta t}\mathbf{v}^{(i-1)}) \mathbf{H} dV \tag{10}$$

$$\mathbf{K_{vp}} = -\int_V \nabla \mathbf{H}^T \mathbf{G} dV$$

$${}^{t+\Delta t}\mathbf{F}_{\mathbf{v}}^{(i-1)} = {}^{t+\Delta t}\mathbf{R_B} + {}^{t+\Delta t}\mathbf{R}_{\mathbf{S}}^{(i-1)} -$$

$$\left({}^{t+\Delta t}\mathbf{K}_{\mathbf{vv}}^{(i-1)} + {}^{t+\Delta t}\mathbf{K}_{\mu\mathbf{v}}^{(i-1)}\right) {}^{t+\Delta t}\mathbf{v}^{(i-1)} - \mathbf{K_{vp}}\, {}^{t+\Delta t}\mathbf{p}^{(i-1)}$$

$${}^{t+\Delta t}\mathbf{F}_{\mathbf{p}}^{(i-1)} = -\mathbf{K}_{\mathbf{vp}}^T\, {}^{t+\Delta t}\mathbf{v}^{(i-1)}$$

$${}^{t+\Delta t}\mathbf{R_B} = \int_V \mathbf{H}^T {}^{t+\Delta t}\mathbf{f^B} dV$$

$${}^{t+\Delta t}\mathbf{R}_{\mathbf{S}}^{(i-1)} = \int_S \mathbf{H}^T \left(-{}^{t+\Delta t}p^{(i-1)}\mathbf{n} + \nabla^{t+\Delta t}\mathbf{v}^{(i-1)} \cdot \mathbf{n}\right) dS$$

The left upper index "t+Δt" denotes that the quantities are evaluated at the end of time step. Also V and S are the volume and the surface of the finite element, respectively. The matrix $\mathbf{H}$ and $\mathbf{G}$ contains the interpolation functions for the velocities and the pressure respectively. The matrix $\mathbf{M}_{\mathrm{v}}$ is mass matrix, $\mathbf{K}_{\mathrm{vv}}$and $\mathbf{J}_{\mathrm{vv}}$ are convective matrices, $\mathbf{K}_{\mu\mathrm{v}}$ is viscous matrix, $\mathbf{K}_{\mathrm{vp}}$ is pressure matrix, and $\mathbf{F}_{\mathrm{v}}$ and $\mathbf{F}_{\mathrm{p}}$ are forcing vectors.

4.2 Penalty formulation

The second is the penalty formulation which has a better conditioning of discretized system and also reduced number of degrees of freedom, since now only the velocities are the unknown variables, [29]. The pressure is eliminated at the element level through the static condensation. For the penalty formulation, we define the incompressibility constraint in the following manner:

$$div\mathbf{v} + \frac{p}{\lambda} = 0 \tag{11}$$

where λ is a relatively large positive scalar so that p/λ is numerically zero for practical purposes.

The incremental-iterative form of the equilibrium equations are

$$\left(\tfrac{1}{\Delta t}\mathbf{M_v} + {}^{t+\Delta t}\mathbf{K}_{\mathbf{vv}}^{(i-1)} + {}^{t+\Delta t}\mathbf{K}_{\mu\mathbf{v}}^{(i-1)} + {}^{t+\Delta t}\hat{\mathbf{K}}_{\mu\mathbf{v}}^{(i-1)} + {}^{t+\Delta t}\mathbf{J}_{\mathbf{vv}}^{(i-1)} + \mathbf{K}_{\lambda\mathbf{v}}\right)\Delta\mathbf{v}^{(i)} = {}^{t+\Delta t}\hat{\mathbf{F}}_{\mathbf{v}}^{(i-1)} \tag{12}$$

c

where the matrices and vectors are

$${}^{t+\Delta t}\hat{\mathbf{K}}_{\mu\mathbf{v}}^{(i-1)} = \int_V \mu\mathbf{H}^T\mathbf{H}dV$$

$$\mathbf{K}_{\lambda\mathbf{v}} = \lambda\int_V \mathbf{H}^T\mathbf{H}dV \tag{13}$$

$${}^{t+\Delta t}\hat{\mathbf{F}}_{\mathbf{v}}^{(i-1)} = {}^{t+\Delta t}\mathbf{R_B} + {}^{t+\Delta t}\hat{\mathbf{R}}_{\mathbf{S}}^{(i-1)} -$$

$$\left({}^{t+\Delta t}\mathbf{K}_{\mathbf{vv}}^{(i-1)} + {}^{t+\Delta t}\mathbf{K}_{\mu\mathbf{v}}^{(i-1)} + {}^{t+\Delta t}\hat{\mathbf{K}}_{\mu\mathbf{v}}^{(i-1)} + \mathbf{K}_{\lambda\mathbf{v}}\right){}^{t+\Delta t}\mathbf{v}^{(i-1)}$$

$${}^{t+\Delta t}\left(\hat{\mathbf{R}}_{\mathbf{S}}\right)_{i\alpha}^{(i-1)} =$$

$$\int_S \mathbf{H}^T\left[\lambda\,{}^{t+\Delta t}\nabla\mathbf{v}^{(i-1)}\cdot\mathbf{n} + \left({}^{t+\Delta t}\nabla\mathbf{v}^{(i-1)} + {}^{t+\Delta t}\nabla^T\mathbf{v}^{(i-1)}\right)\cdot\mathbf{n}\right]dS$$

Additional matrices from velocity-pressure formulation here are denote with'" and the other matrices and vectors are the same as in equation (10).

4.3 Coupling with mass transport

In coupling of the blood flow with the mass transport we have domination of the convection terms due to the low diffusion coefficient. Then it is necessary to have special stabilizing techniques in order to obtain a stable numerical solution.

Here we have implemented the streamline upwind/Petrov-Galerkin stabilizing technique (SUPG), [30]. This stabilizing scheme is used in the weighted residual formulation, applied in the direction of the streamlines, only.

The incremental-iterative form of equations is

$$\begin{bmatrix} a & \mathbf{K_{vp}} & \mathbf{0} \\ \mathbf{K_{vp}^T} & \mathbf{0} & \mathbf{0} \\ {}^{t+\Delta t}\mathbf{K}_{cv}^{(i-1)} & \mathbf{0} & b \end{bmatrix} \begin{Bmatrix} \Delta\mathbf{v}^{(i)} \\ \Delta\mathbf{p}^{(i)} \\ \Delta\mathbf{c}^{(i)} \end{Bmatrix} = \begin{Bmatrix} {}^{t+\Delta t}\mathbf{F}_{\mathbf{v}}^{(i-1)} \\ {}^{t+\Delta t}\mathbf{F}_{\mathbf{p}}^{(i-1)} \\ {}^{t+\Delta t}\mathbf{F}_{c}^{(i-1)} \end{Bmatrix} \tag{14}$$

$$a = \frac{1}{\Delta t}\mathbf{M_v} + {}^{t+\Delta t}\mathbf{K}_{\mathbf{vv}}^{(i-1)} + {}^{t+\Delta t}\mathbf{K}_{\mu\mathbf{v}}^{(i-1)} + {}^{t+\Delta t}\mathbf{J}_{\mathbf{vv}}^{(i-1)}$$

$$b = \frac{1}{\Delta t}\mathbf{M}_c + {}^{t+\Delta t}\mathbf{K}_{cc}^{(i-1)} + {}^{t+\Delta t}\mathbf{J}_{cc}^{(i-1)}$$

where the matrices and vectors are

$$\mathbf{M} = \rho\int_V \mathbf{H}^T\mathbf{H}dV \quad {}^{t+\Delta t}\mathbf{K}_{cv}^{(i-1)} = \rho\int_V \mathbf{H}^T\mathbf{H}^{t+\Delta t}\mathbf{c}^{(i-1)}\mathbf{H}dV$$

$${}^{t+\Delta t}\mathbf{K}_{cc}^{(i-1)} = \int_V k\mathbf{H}^T\mathbf{H}dV \quad {}^{t+\Delta t}\mathbf{J}_{cc}^{(i-1)} = \rho\int_V c_p\mathbf{H}^T\mathbf{H}^{t+\Delta t}\mathbf{v}^{(i-1)}\mathbf{H}dV$$

$${}^{t+\Delta t}\mathbf{F}_c^{(i-1)} = {}^{t+\Delta t}\mathbf{F}_q + {}^{t+\Delta t}\mathbf{F}_{sc}^{(i-1)} - \tfrac{1}{\Delta t}\mathbf{M}_c\left\{{}^{t+\Delta t}\mathbf{c}^{(i-1)} - {}^{t}\mathbf{c}\right\} -$$

$${}^{t+\Delta t}\mathbf{K}_{\mathbf{cv}}^{(i-1)}\left\{{}^{t+\Delta t}\mathbf{v}^{(i-1)}\right\} - {}^{t+\Delta t}\mathbf{K}_{cc}^{(i-1)}\left\{{}^{t+\Delta t}\mathbf{c}^{(i-1)}\right\}$$

$$^{t+\Delta t}\mathbf{F}_q = \int_V \mathbf{H}^T q^B dV \quad ^{t+\Delta t}\mathbf{F}_{sc}^{(i-1)} = \int_S k\mathbf{H}^T \nabla^{t+\Delta t}\mathbf{c}^{(i-1)} \cdot \mathbf{n} dS \qquad (15)$$

The matrix $\mathbf{K}_{\mathrm{cc}}$ is mass matrix for gas-concentration, $\mathbf{K}_{\mathrm{cv}}$ and $\mathbf{J}_{\mathrm{cc}}$ represent convective part of equation (7), and $\mathbf{F}_{\mathrm{c}}$ is forcing vector for convection diffusion equation (7).

5 Computational Results

After the FE analysis is completed, the user-surgeon has many options to look at the results. We give here only part of the results, which are the most commonly presented in the literature. Some authors, as reference [3], analyzed the results for specified pulse phase angles during the pulse cycle. These phase angles are:

systolic peak flow, $\mathrm{t/t_p}$=0.10

systolic deceleration flow, $\mathrm{t/t_p}$=0.125

diastolic minimum flow, $\mathrm{t/t_p}$=0.325

diastolic flow, $\mathrm{t/t_p}$=0.775.

5.1 Velocity field

The velocity fields in the branching plane at different pulse phase are shown in Fig.8, [31-33].

There is a clear identification of stagnation flow zone in the carotid sinus (cross-sections C,D and E from Fig. 1). The black color denotes zero or less then zero velocity and in these sites are the most possible growing of the atherosclerosis if patient has already beginning stadium of

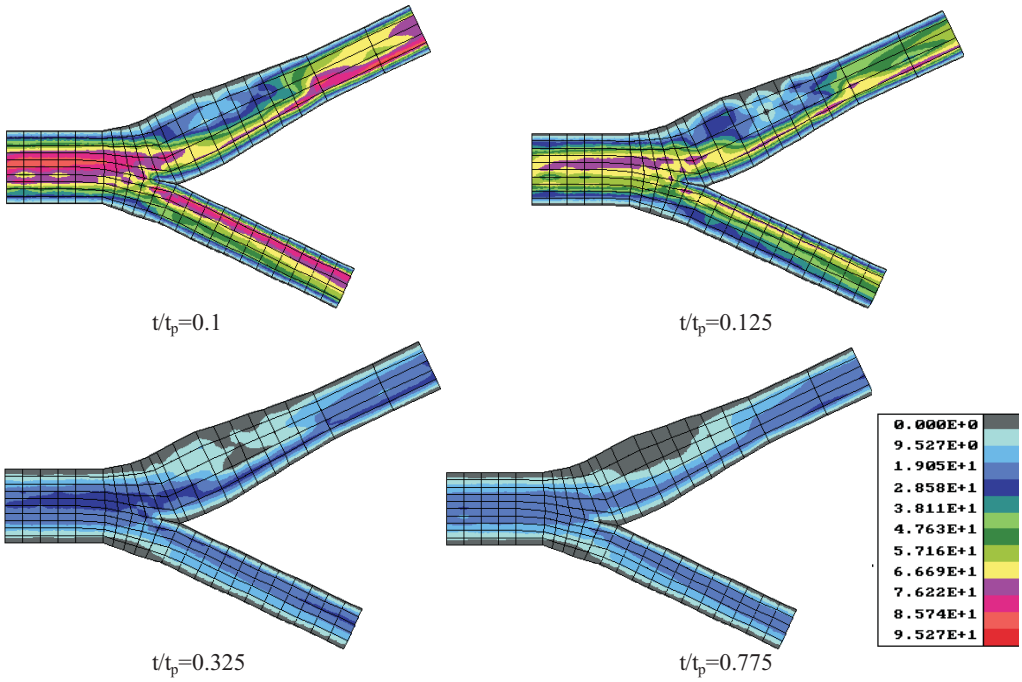

Figure 8: The velocity field in the branching plane at different pulse phase

this disease. It can be seen that this stagnation flow is observed almost in all the specified pulse phase angles during the pulse cycle. The units associated with the color figures are cm/s for effective velocity.

The 3D velocity field at the diastolic flow is presented in Fig. 9. User can choose any viewpoint for the 3D model. The variables, which can be on the display, are velocity, pressure and the wall shear stress. The velocity can be presented by the profiles at selected cross-sections, or as a vector field at all (selected) nodes. Also the velocity field can be displayed in the color mode, where each color denotes an interval (linear or logarithm) for intensity of the velocity vectors. A classical Doppler ultrasound and magnetic resonance imaging could be significant improve with this software. The reason is because there is no such precision in the velocity field in these classical medical diagnostic device as it is presented in the virtual numerical simulation.

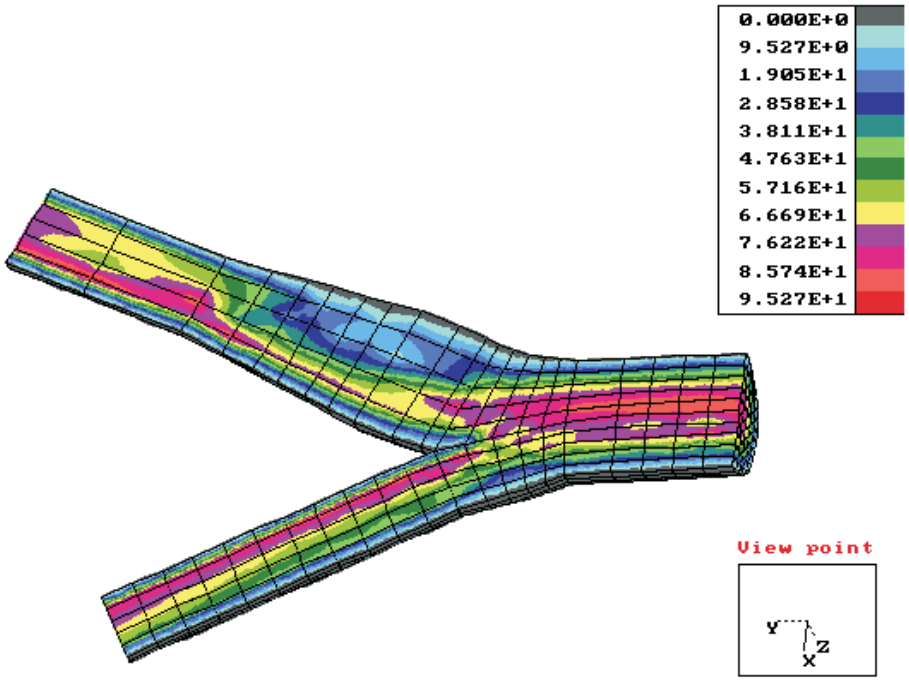

Figure 9: 3D velocity field at the diastolic flow

a) Axial velocity (t/t_p=0.125)

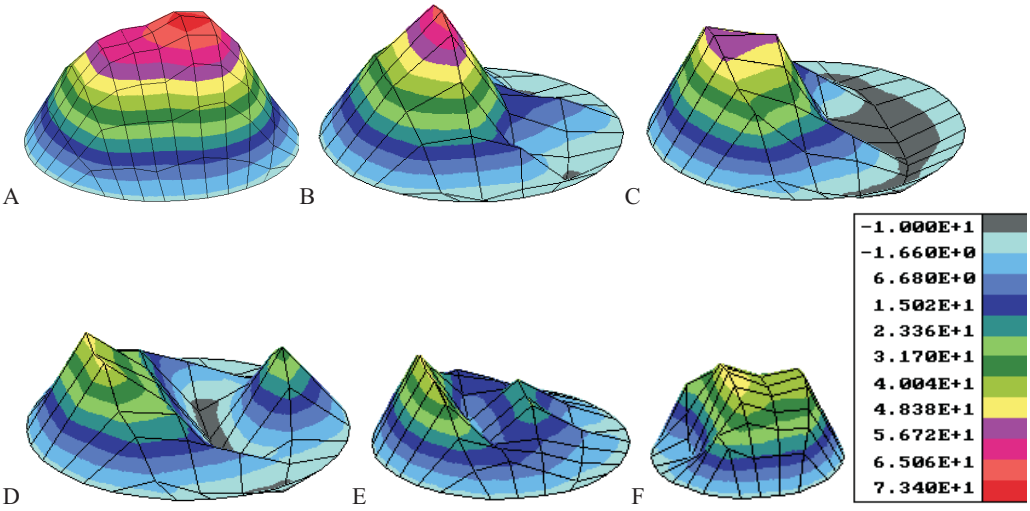

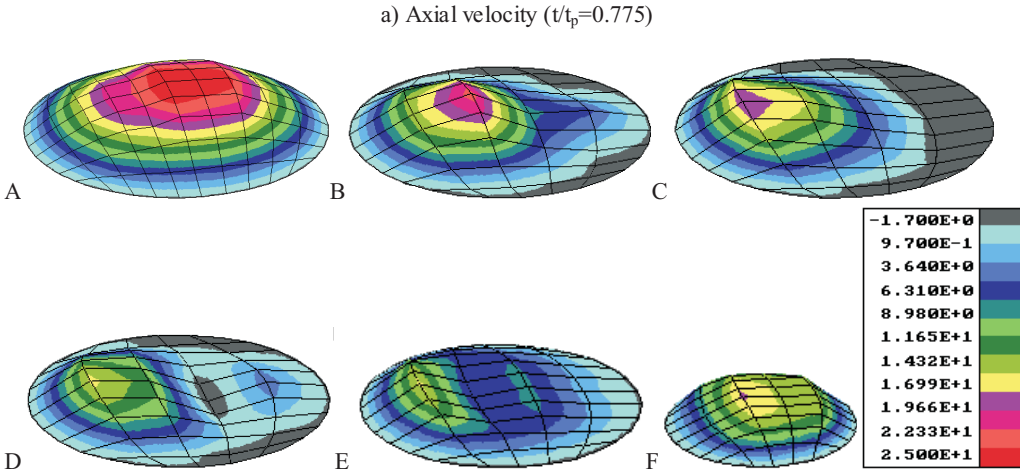

a) Three-dimensional representation of axial velocity field
b) Secondary flow velocity field and vector plots

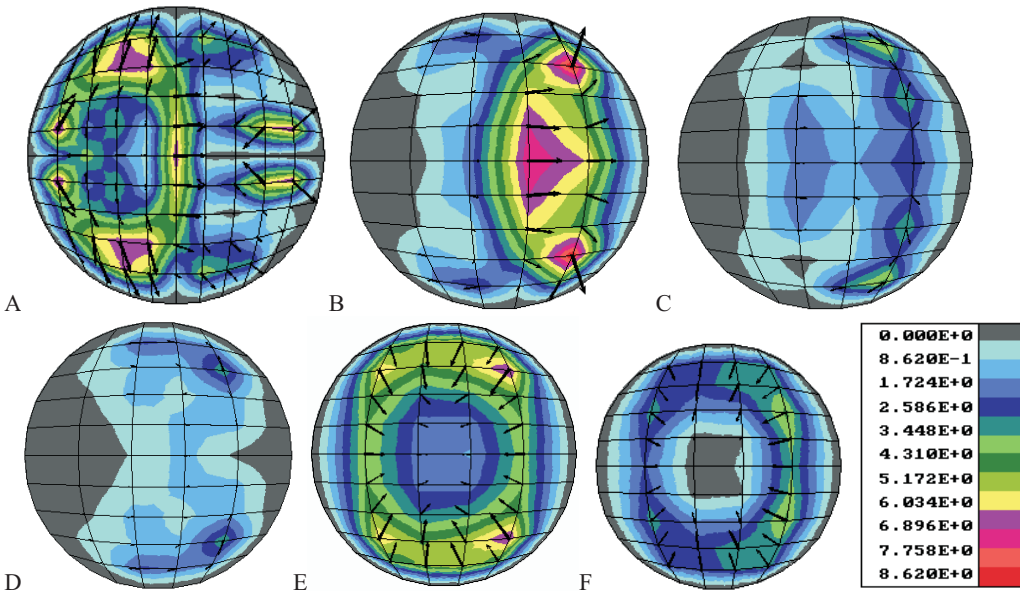

Fig. 10 displays three-dimensional representation of axial and secondary velocity field for systolic deceleration and diastolic phase at different locations. There is obviously the reverse flow in the cross-section C, D and E during systolic deceleration flow, t/t_p=0.125. Also dur-

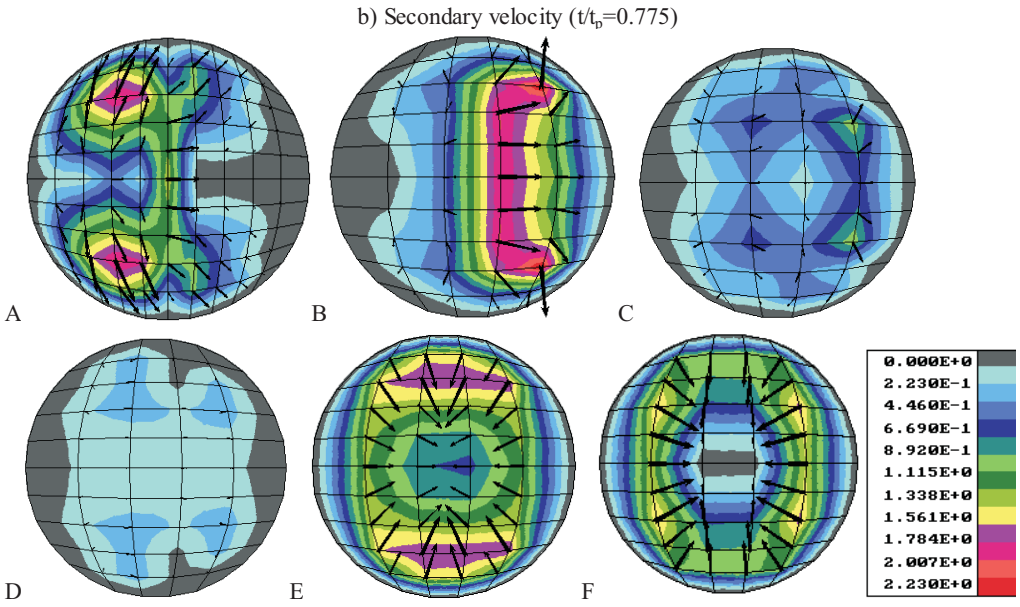

Figure 10: Three-dimensional representation of the axial and secondary velocity fields for systolic deceleration (t/t_p=0.125) and diastolic phase (t/t_p=0.775), at different locations indicated in Fig. 1

c) Three-dimensional representation of axial velocity field
d) Secondary flow velocity field and vector plots

ing much longer diastolic flow the recirculation flow is dominant at the cross-section B,C, and D from Fig. 1. The secondary flow in these two characteristics phases shows strong recirculation. The finer finite element mesh should give more clearly figure about these recirculation secondary flows.

5.2 The blood pressure

The pressure distributions in the branching plane at different pulse phases are shown in Fig. 11. One of the characteristics of the bifurcation flow is the stagnation point at the flow divider, which can be

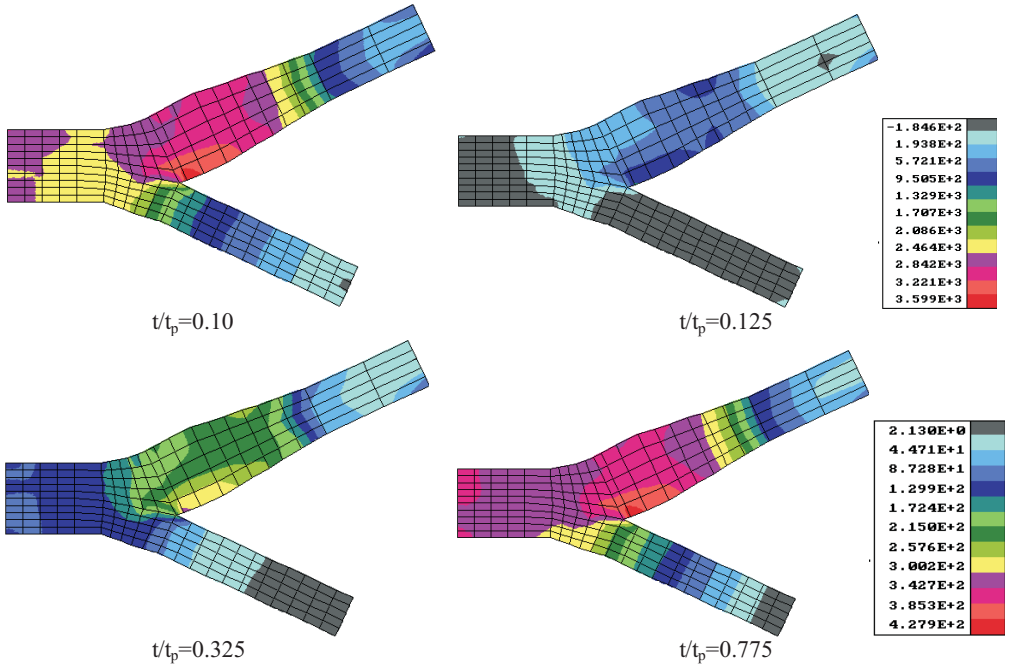

Figure 11: The pressure distribution in the branching plane at different pulse phases

identified in the displayed numerical solutions. The pressure is not usual presented in the numerical results due to difficulty to determine it from calculation. Non-stability of the fluid pressure was solved by penalty formulation and these results are obtained using post-processing fluid flow velocity results.

5.3 Wall shear stresses

The wall shear stress is proportional to the shear rate γ at the wall, and the fluid dynamic viscosity μ. The measurements of the velocity gradient near the wall is technically difficult. The gradient depends highly on the shape of the velocity profile and on the measurement accuracy of distance from the wall. The endothelial cells respond to shear stress. At the lumenal surface, the shear stress can be sensed directly as a force on an endothelial cell.

Arteries adapt to long-term increases or decreases in wall shear stress. For example, decreased flow rates will cause a thickening of the intimal layer to reestablish a normal wall shear stress. On the other hand, increased wall shear stress is a responce to remodeling arteries to a large diameter, as it is observed through creation of an arteriovenous fistula for hemodialysis access. The medial thickness is influenced by the local amount of the hoop stress and nutrition. It is known that the hoop stress will proportionally increase as the blood pressure increases. Alterations in the pulsatile pressure lead to changes in organization of the elastin and collagen structure within the media. One of the direct consequences of the low shear stress is acceleration of the intimal thickening. There are many pathological states which can arise from an excessive or uncontrolled response to a hemodynamic effects.

It follows from the above facts that determination of the shear stress field is very important. The FE analysis provides the accurate calculation of the wall shear stresses in complex blood flow patterns. Examples of the shear stress fields are shown in Fig. 12. It can be observed that wall shear stress is very low during diastolic flow. This is directly in correlation with danger zone of possible chemical interaction within the endothelial cells. Also it is very important to calculate oscillating wall shear stress (not presented here) in order to predict the development of the atherosclerotic diseases.

5.4 Hemodynamics of stenosis

Shear rate increases rapidly in the converging stenosis, reaching a peak just upstream of the throat. In the post-stenotic recirculation region the shear rate is low and negative. The process of collapse in the stenotic arteries induces a compressive stress that can buckle the artery walls. Also, oscillations in compressive loading can create a fracture fatigue in the surface of the atheroma, causing a rupture of the plaque cap.

Some authors, as reference [34], studied the intraluminal throumbus within the abdominal aortic aneurysm which can serve as a barrier to oxygen diffusion from the lumen to the inner layers of the aortic wall. This may lead to hypoxia, which may further cause the wall weakening and increased potential for rupture. As it is very difficult to determine

the diffusion coefficient, especially for each patient, the numerical simulation can improve the understanding all these phenomena.

The shifts in flow velocity maxima indicate that the shear stress is higher along the inner wall of the carotid sinus than at the outer wall. Also, for normal physiological conditions, the shear stresses are higher along the flow divider than in the common carotid, and the shear stress values are much higher in the distal internal carotid than in the common carotid artery, see Fig. 12. The intensity of shear stress is inversely proportional to the distribution of the intimal thickness in the specimens, [13].

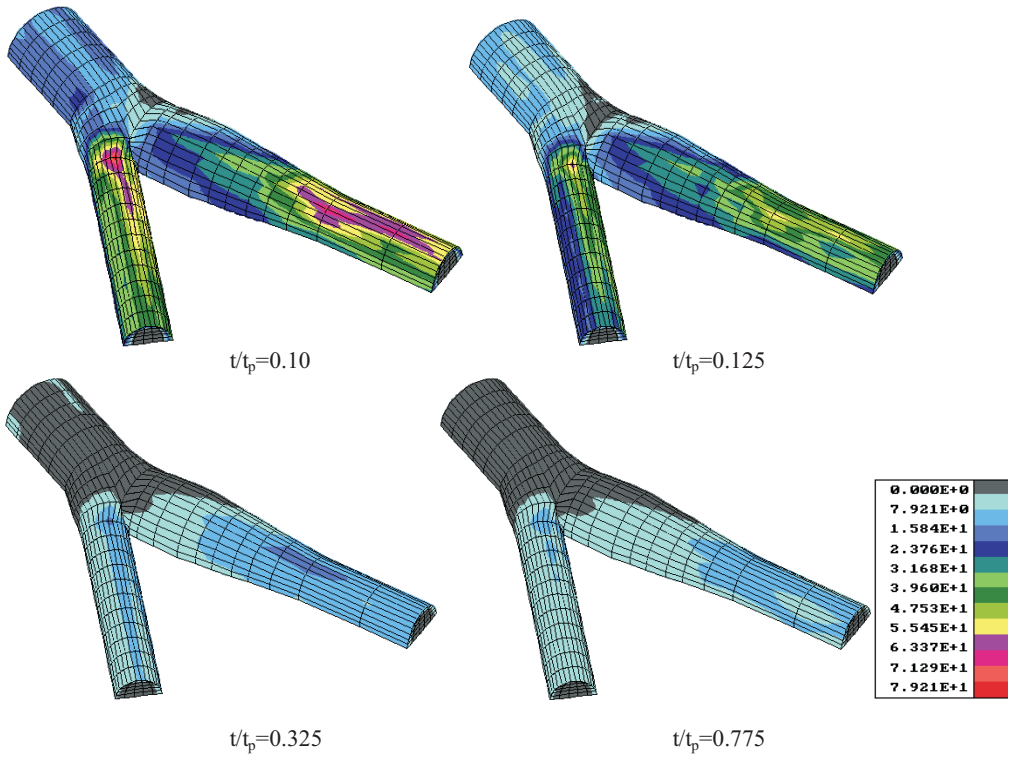

Figure 12: Wall shear stress field at different pulse phases

Distribution of oxygen concetration in carotid artery bifurcation for t/t_p=0.125 is shown in Fig. 13. There are a few separation regions at the outer wall which indicate the combined effect of fluid boundary layer

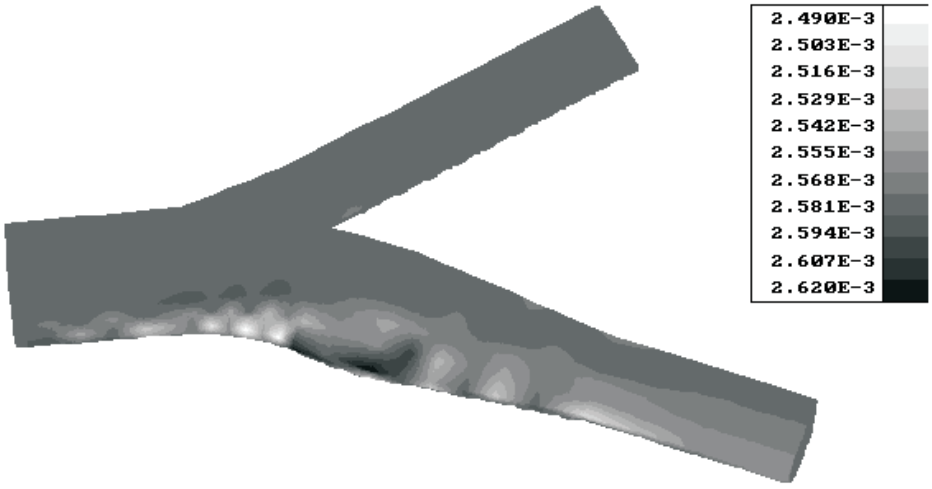

Figure 13: Distribution of oxygen concentration in carotid artery bifurcation for t/t_p=0.125

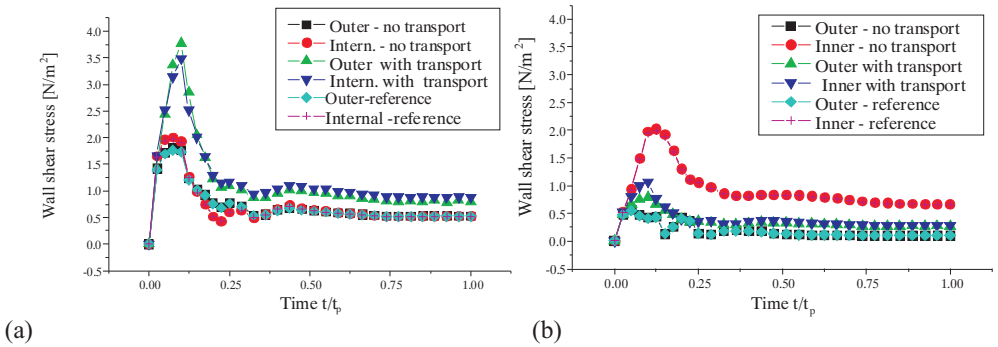

Figure 14: Wall shear stress vs pulse phase angle at the outer wall and at the inner wall for locations A, and D indicated in Figure 1 (with and without transport of oxygen

(a) Location A: common carotid
(b) Location D: maximum carotid sinus

resistance and endothelial resistance.

Fig. 14 shows the wall shear stress vs pulse phase angle at the outer

wall and at the inner wall, for the location A and D indicated in Fig. 1, and without and with oxygen transport. The results illustrate an essential influence of the oxygen transport on the blood flow. For the cross-section A from Fig. 1 the wall shear stress is higher with using coupled transport equation and in the cross-section D (maximum carotid sinus) with transport equation the wall shear stress is lower.

6 Discussion

As already mentioned, this work offers a first-generation vascular-surgical simulation for the carotid artery bifurcation. It requires vascular surgeons should be quite familiar with computers, and with computational mechanics to interpret the results of the output data generated by this software. This is a limitation of the current system because any surgical software simulation must be easy to use and to interpret the clinical significance of the results. An additional work is necessary to produce a system that performs well in this respect.

A second limitation is the amount of time required to complete the simulation. Each of the simulations for the today's capacity of PC computers requires about 12 hours of run-time for 3 cycles. The current hardware precludes the surgeon from interacting in real-time with the simulation. With the rapidly-increasing speed of computers the real-time runs should be possible in the near future.

One of the possibilities to make the software usable with the today's hardware is to implement the parallel computing. Parallel processing is often used for the analysis of large scale problems. For this purpose a model is decomposed into subdomains and the analysis is performed on each subdomain by one processor. The solutions are condensed and combined for the overall solutions, leading to a drastic reduction of the computing time.

From the clinical aspects, it is difficult to develop a universal expert system for diagnostic purposes. The above discussion indicate some possibilities in this direction. A schematic representation of a future expert system is shown in Fig. 15. After a few geometrical measurements from medical device such as Doppler ultrasound, CAD systems of software provide automatic solid model which goes to automatic finite element

mesh and numerical calculations. After many numerical, experimental and clinical studies this expert system should have a large database on which some artificial inteligence system (nerual network, fuzzy logic, genetic algorithm, etc.) could be applied. The medical doctor is not excluded through this software process, even more he is now much more oriented to clinical aspects and predictive medicine rather rutine clinical examinations.

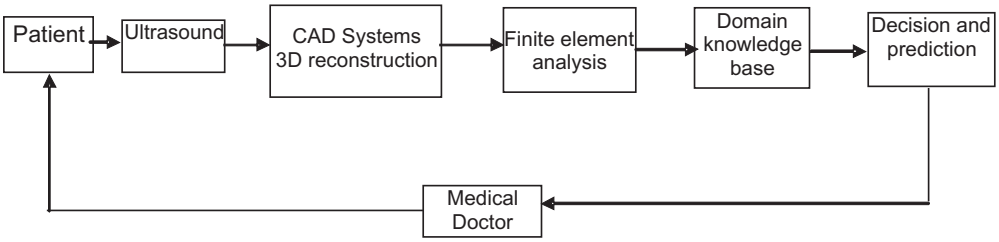

Figure 15: Expert system for making decision in predictive medicine

7 Conclusion

The major topic addressed in this paper is to present computational techniques which could enable pysicians to diagnostic and design patient-specific treatment plans that improve their care. For this purpose it is developed a software system for the carotid bifurcation artery to integrate: definition of geometry, automatic mesh generation, boundary and initial conditions, three-dimensional flow with mass transfer solution and scientific visualization. Since the developed software is of the object-oriented type, other computer programs could replace the current componental parts. This practically means that it is possible to easily develop a modul for other human vascular vessels.

The results shown here for velocity, pressure and shear stress are in the good agremeent with every day clinical work. Also a specific coupled finite element fluid flow system with transport equation is presented.

The clinical application of the numerical modeling and development of predictive methods will occupy scientists for many years to come.

With the predictive medicine paradigm proposed herein, a physician could simulate a surgical procedure and even more implement and quantitatively evaluate alternate treatment plans using simulation-based software expert system. This computer aided surgical planning would not be possible for vascular surgery if it takes days or weeks to create computationl models. With the proposed approach it is possible to create these models in minutes or hours. With a use of parallel computing and specific numerical techniques, the clinically relevant problems can be analyzed in real time. These computatinal methods can improve patient care with knowledge of the effect of hemodynamic conditions on vascular adaptation and disease, and the determination of the optimal hemodynamic condtions for an individual patient. It is important to note that the information provided by the computer simulations of blood flow provides only a portion of data which are needed to design a treatment plan. Numerous other factors, including the morbidity and mortality of the procedure, must be considered. Anyway we are thinking that computer simulation will have important applications in the medicine of the future.

References

[1] D.E. Strandness, and B.C. Eikelboom, (1998), Carotid artery stenosis – where do we go from here?, *European Journal of Ultrasound,* **7**, 17-26.

[2] K. Perktold, M. Resch, and O. Peter, (1991), Three-dimensional numerical analysis of pulsatile flow and wall shear stress in the carotid artery bifurcation model, *J. Biomechanics*, **24**, 409-420.

[3] K. Perktold, R. O. Peter, M. Resch, and G. Langs, (1991), Pulsatile non-Newtonian blood flow in three-dimensional carotid bifurcation models: a numerical study of flow phenomena under diferent biurcation angles, *J. Biomech. Engrg.*, **13**, 507-515.

[4] K. Perktold, M. Resch, and H. Florian, (1991), Pulsatile non-Newtonian flow characteristics in a tree-dimensional human carotid bifurcation model, *J. Biomech. Engrg.*, **113**, 464-475.

[5] K. Perktold, E. Thurner, and T. Kenner, (1994), Flow and stress characteristics in rigid walled and compliant carotid artery bifurcation models, *Medical & Biological Engineering& Computing*, **32**, 19-26.

[6] K. Perktold, and G. Rappitsch, Computer simulation of arterial blood flow, Vessel diseases under the aspect of local haemodynamics, *Biological flow*, eds. M.Y. Jaffrin and C. Caro, (Plenum press, New York, 1994).

[7] K. Perktold, and G. Rappitch, (1995), Computer simulation of local blood flow and vessel mechanics in a compliant carotid artery bifurcation model, *J. Biomechanics*, **28**, 845-856.

[8] K. Perktold, M. Hofer, G. Rappitsch, M. Loew, B.D. Kuban, and M.H. Friedman, (1998), Validated computation of physiologic flow in realistic coronary artery branch, *J. Biomechanics*, **31**, 217-228.

[9] K. Perktold, M. Hofer, G. Karner, W. Trubel, and H. Schima, Computer simulation of vascular fluid dynamics and mass transport: Optimal design of arterial bypass anastomoses, ECCOMAS 98, *Computational hemodynamics*, (John Wiley& Sons, 1998).

[10] C.C.M. Rindt, A.A. van Steenhoven, J.D. Janssen, R.S. Reneman, and A. Segal, (1990), A numerical analysis of steady flow in a three-dimensional model of the carotid artery bifurcation, *J. Biomechanics*, **23**, 461-473.

[11] C.A. Taylor, T.J.R. Hughes and C.K. Zarins, (1998), Finite element modeling of blood flow in arteries, *Comput. Meths. Appl. Mech. Engrg.*, **158**, 155-196.

[12] B.K. Bharadvej, R.F. Maron, and D.P. Giddens, (1982), Steady flow in a model of the human carotid bifurcation. Part I-flow visuelisation, *J. Biomechanics*, **15**, 349-362.

[13] C.K. Zarins, D.P. Giddens, B.K. Bharadvej, V.S. Sottiurai, R.F. Mabon, and S. Glagov, (1983), Carotid bifurcation ahterosclerosis: Quantitative correlation of plaque localization with low velocity profiles and wall shear stress, *Circ. Res.*, **53**, 502-514.

[14] D.N. Ku, D.P. Giddens, C.Z. Zarins, and S. Glagov, (1985), Pulsatile flow and arterosclerosis in the human carotid bifurcation, *Arteriosclerosis*, **5**, 293-302.

[15] D.N. Ku, and D.P. Giddens, (1987), Laser Doppler anemometer measurements of pulsatile flow in a model carotid bifurcation, *J. Biomechanics*, **20**, 407-421.

[16] D.N. Ku, (1997), Blood flow in arteries, *Annu. Rev. Fluid Mech.*, **29**, 399-434.

[17] S.Z. Zhao, X.Y. Xu, M.W. Collins, A.V. Stanton, A.D. Hughes, and S.A. Thom, (1999), Flow in carotid bifurcations: effect of the superior thyroid artery, *Medical Engineering & Physics*, **21**, 207-214.

[18] A. Delfino, N. Stergiopulos, J.E. Moore, Jr and J.-J. Meister, (1997), Residual strain effects on the stress field in a thick wall finite element model of the human carotid bifurcation, *J. Biomechanics*, **30**, 777-786.

[19] D.M. Wootton, D.N and Ku, (1999), Fluid mechanics of vascular systems, diseases, and thrombosis, *Annu. Rev. Biomed. Eng.* , **1**, 299-329.

[20] G. Schneiderman, C.G. Ellis, and T.K. Goldstick, (1979), Mass transport to walls of stenosed arteries: variation with Reynolds number and blood flow separation, *J. Biomechanics*, **12**, 869-877.

[21] G. Rappitsch, and K. Perktold, (1996), Computer simulation of convective diffusion processes in large arteries, *J. Biomechanics*, **29**, 207-215.

[22] N. Filipovic, *Structural Analysis by FEM with Automatic Grid Generation*, B. S. Thesis, Faculty of Mechanical Engineering, (Kragujevac, Serbia-Yugoslavia, 1994)

[23] Y.J. Cho, and K.R. Kensey, (1991), Effects of the non-Newtonian viscosity of blood on flows in a diseased arterial vessel. Part 1: Steady flow*, Biorheology* , **28**, 241-262.

[24] J.A. Moore, and C.R. Etheir, (1997), Oxygen mass transfer calculations in large arteries, *J. Biomech. Engrg.*, **119**, 469-475.

[25] M. Kojic, R. Slavkovic, M. Zivkovic, and N. Grujovic, *Finite Element Method I* (in Serbian), Faculty of Mech. Engrg., (Univ. Kragujevac, Serbia-Yugoslavia, 1998)

[26] N. Filipovic, *Numerical Analysis of Coupled Problems: Deformable Body and Fluid Flow*, Ph. D. Thesis, Faculty of Mechanical Engineering, Kragujevac, (Serbia-Yugoslavia, 1999).

[27] M. Kojic, N. Filipovic, M. Zivkovic, R. Slavkovic, and N. Grujovic, *PAK-F Finite Element Program for Laminar Flow of Incompressible Fluid and Heat Transfer*, Laboratory for Engineering Software, Faculty of Mech. Engrg, Univ. Kragujevac, (34000 Kragujevac, Serbia-Yugoslavia, 1999)

[28] P.M. Gresho, R.L., Lee, and R.L. Sani, On the time dependent solution of the incompressible Navier-Stokes equations in two and three dimension, Chapter 2, *Finite Elements in Fluids*, Vol. 4, (eds. Gallagher et al., John Wiley & Sons, Chichester, 1982).

[29] N. Filipovic, *Numerical Analysis of Coupled Problems: Fluid Flow Through Porous Deformable Medium with Implementation in Biomechanics and Geomechanics*, Candidate Report for Ph.D. Thesis, Faculty of Mechanical Engineering, (Kragujevac, Serbia-Yugoslavia, 1996).

[30] A.N. Brooks, T.J.R and Hughes, (1982), Streamline upwind/Petrov-Galerkin formulations for convection dominated flows with particular emphasis on the incompressible Navier-Stokes equations, *Comput. Meths. Appl. Mech. Engrg.*, **32**, 199-259.

[31] N. Filipovic, M. Kojic, B. Novakovic, and M. Rosic, (1999), Computer simulation of mass transport in large arteries with wall deformation. *In Proceedings of the 6th International Conference for Medical Physics*, Patras, Greece .

[32] M. Kojic, B. Novakovic, and N. Filipovic, (1999), Computational hemodynamics in a carotid artery bifurcation model, *In Proceedings of the 6th International Conference for Medical Physics*, Patras, Greece.

[33] M. Kojic, and K.J. Bathe, (2001), *Inelastic Analysis of Solids and Structures*, Springer-Verlag, Berlin/Heidelberg (to be published).

[34] D.A. Vorp, D.H.J. Wang, M.W. Webster and W.J. Federspiel, (1998), Effect of intraluminal thrombus thickness and bulge diameter on the oxygen diffusion in abdominal aortic aneurysm, *Journal of Biomechanical Engineering*, **120**, 579-583.

Submitted on March 2004, revised on May 2004.

Kompjuterske simulacije protoka krvi transporta mase kroz bifurkaciju karotidne arterije

UDK 532.528

Klinička dijagnostika vaskularnih bolesti današnjice zasniva se na dijagnostici medicinskih slika koje predstavljaju trenutno stanje pacijenta i iskustvenim procenama koje uzimaju u obzir efikasnost odgovarajućih tretmana kod sličnih slučajeva. Ove tehnike su nedovoljne za predvidjanje posledica datih tretmana za svakog individualnog pacijenta. U ovom radu predlažemo novi koncept gde lekari mogu koristiti kompjuterske simulacije da naprave model sa specifičnim geometrijskim karakteristikama i da predvide posledice za svakog individualnog pacijenta.

Za takav koncept neophodno je razviti složen softverski sistem koji obuhvata korisničke interfejse, automatske generatore mreža konačnih elemenata, kompjutersko modeliranje dinamike fluida i postprocesorske vizualizacije.

Dinamika fluida je opisana nestišljivim Navije-Stoksovim jednačinama za Njutnov i ne-Njutnov fluid. Transport mase kiseonika i makromolekula je modeliran konvektivno-difuznom jednačinom i izvršena je sprega sa kretanjem fluida. Kompjuterske simulacije su zasnovane na metodi konačnih elemenata gde su opisani novi metodi sprezanja transporta kiseonika i strujanje fluida.

Rezultati poredjenja pokazuju dobro slaganje sa lokacijama kritičnih zona odvajanja strujanja, recirkulaciji strujanja, male vrednosti smičućeg napona, to sve može značajno doprineti razvoju arterioskleroze.